Supporting Information

Multi-layer nanoarrays sandwiched by anodized aluminium oxide membranes: approach to inexpensive, reproducible, highly sensitive SERS substrate

Chengchun Zhao[a], Yuan Zhu*[a,b], Li Chen*[b], Shaoxin Zhou[a], Yuquan Su[c], Xu Ji[c], Anqi Chen[a], Xuchun Gui[c], Zikang Tang[d], and Zhaowei Liu[c]

[a] *College of Innovation and Entrepreneurship, Southern University of Science and technology, Shenzhen 518055, China. E-mail: zhuy3@sustc.edu.cn*

[b] *Department of Electrical and Computer Engineering, University of California, San Diego, La Jolla, California 92093, USA. E-mail: yili.fchen@gmail.com*

[c] *State Key Lab of Optoelectronic Materials and Technologies, School of Electronics and Information Technology, Sun Yat-sen University, Guangzhou, 510275, P. R. China.*

[d] *The Institute of Applied Physics and Materials Engineering, University of Macau, Avenida da Universidade, Taipa, Macau, China*

Fabirication details

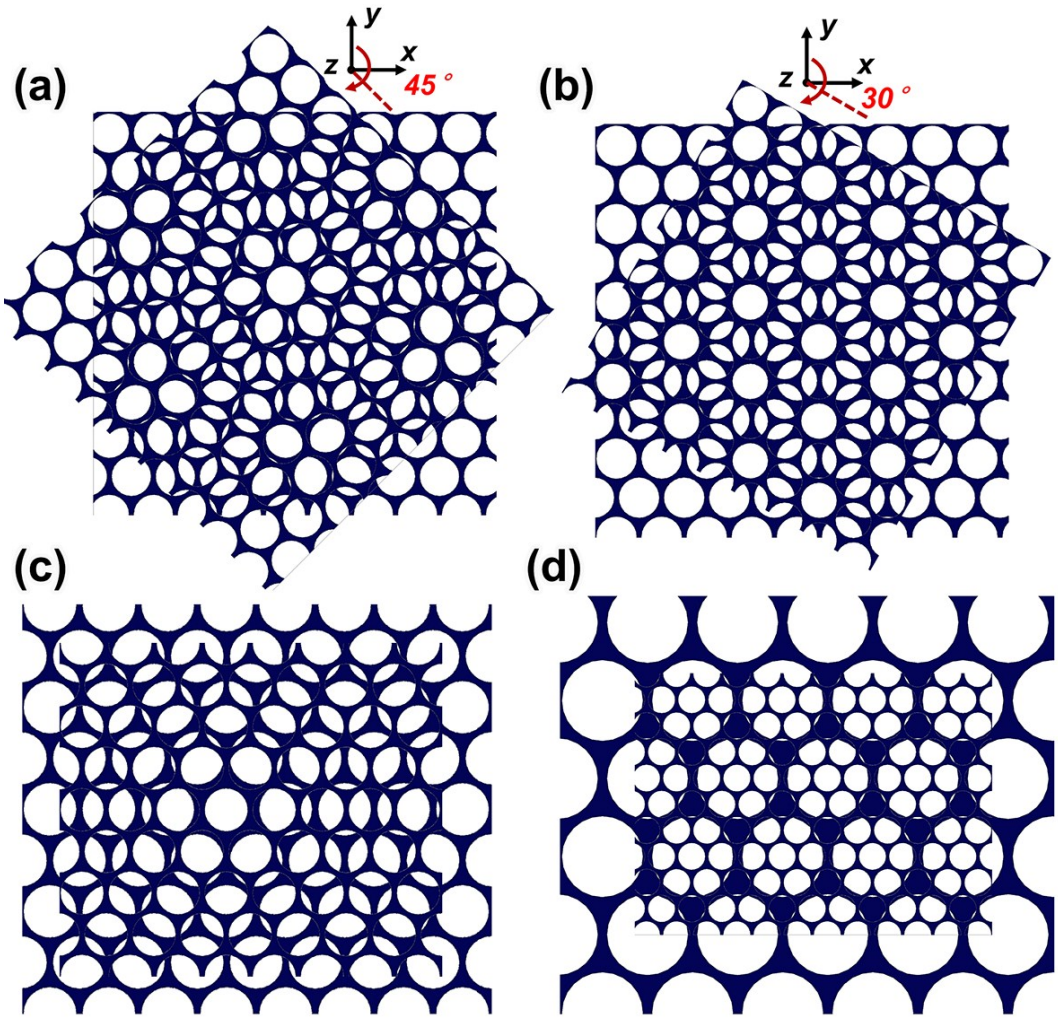

Fig. S1 Relative to the bottom membrane layer, upper layer (a) rotates 45° clockwise. If the upper layer AAO has different pore sizes, its shift and rotation can provide more variations, such as (b) slightly smaller pores and 30° clockwise rotation; (c) slightly smaller pores to fabricate radiative gradient materials; (d) much smaller pores.

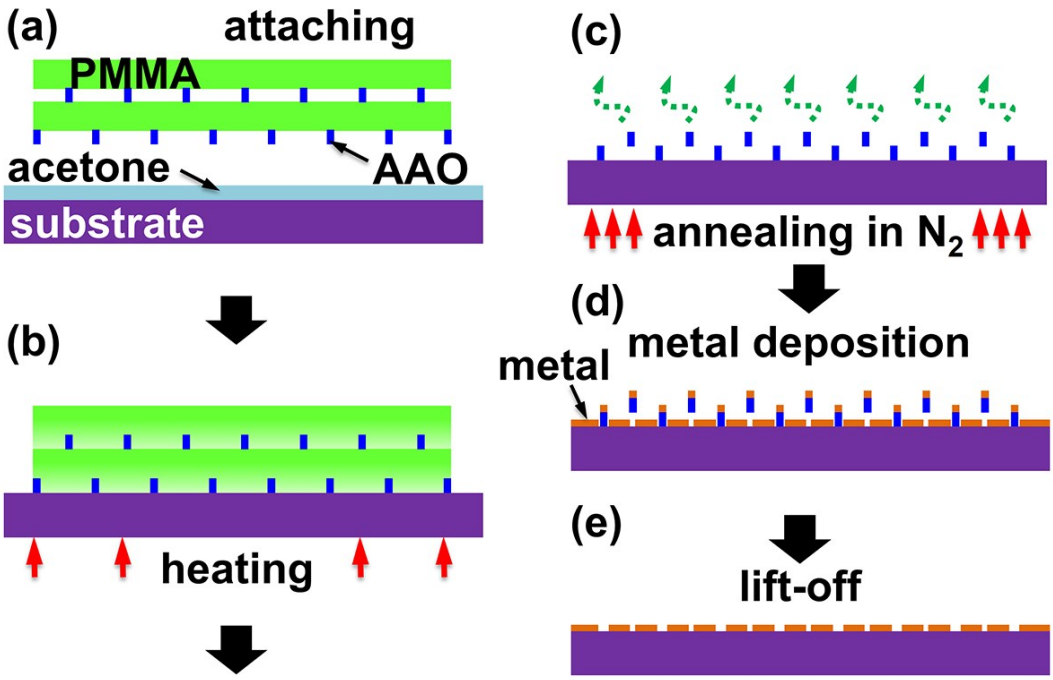

Fig. S2 Schematic outline of the fabrication processes. (a-c) transfer of double layer AAO membranes, (d) metal deposition, (e) lift-off.

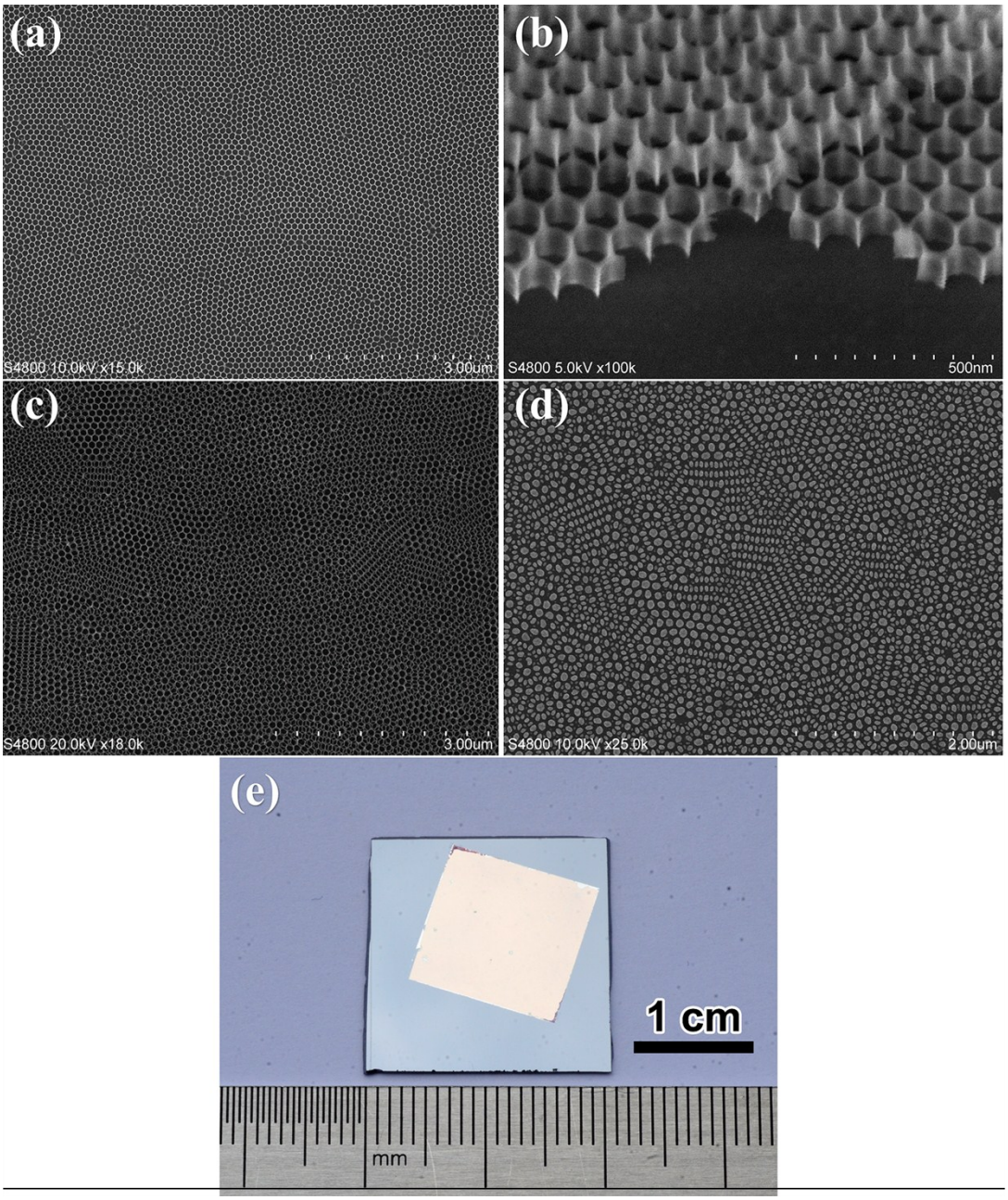

Fig. S3 (a) Low-magnification top-view SEM image of AAO membrane used in this work. (b) 30°-tilted-view SEM images of double AAO membranes. (c) Low-magnification top-view SEM image of the stacked AAO membranes. (d) Low-magnification top-view SEM image of the Ag nanoparticle arrays fabricated by the stacked AAO membranes. (e) Optical image of a large scale Ag nanoparticle arrays on Si wafer after the removal of the double-layer AAO membranes.

In practice, when the AAO membrane is thinner than 200 nm and when its pore wall size is less than 15 nm, the transfer process will be a huge challenge.[1] Although with the support of organic layer, the fragile membrane may be more robust,[2] the additional organic layer removal process yet increases the chance for cracking, wrinkling or folding. Here poly(methyl

methacrylate) (PMMA) is commonly used to assist the transfer of ultrathin AAO membrane, but during the acetone bath, AAO was apt to crack or fold under the convection of acetone and detach from or wrinkle on the substrate because of the weak adhesion. In this work, we present a method that enables the reliable transfer of ultrathin AAO membranes with ~10 nm pore walls over large areas (square cm) based on thermal decomposition of PMMA.

Briefly, a thin acetone layer is first coated on substrate followed by the attaching of PMMA/AAO film (Fig. S2a). The acetone layer prevents the formation of air bubbles between PMMA/AAO and substrate. Once there is a bubble beneath PMMA/AAO film, it expands in heat treatments (Fig. S2b) and hence damages AAO membrane. After the acetone evaporation, part of the PMMA film is dissolved and the remaining part is firmly adhered to the substrate. The substrate is then heated at temperature a little higher than the glass transition temperature of PMMA in order to allow the wavy and rough PMMA/AAO film to make full and flat contact with the target substrate (Fig. S2b). Thanks to the good thermostability of AAO membranes, PMMA can be removed by thermal decomposition (Fig. S2c). The thermal decomposition of PMMA is not affected by atmosphere (such as nitrogen, argon or vacuum), and the predominant product is monomer MMA (> 90%). Besides, products such as CO, CO_2, OH, and CH_4 are formed simultaneously.[3] As shown in Fig. S3a-c, the unbroken and clean surface of AAO membrane indicates the effectiveness of the annealing process for removing PMMA. Annealing at higher temperatures than 400 ^{o}C requires shorter time to remove PMMA completely. Noble gases or vacuum can also be used instead of N_2 in this process.

The pores have a hexagonal shape with round corners, and the pore wall thickness is about 10 nm (Fig. 1a). Fig. 1e-f are their corresponding double layer AAO membranes of the patterns in Fig. 1b-d observed in our experiment. Fig. 1h-j gives the SEM images of their corresponding Ag nanoparticle arrays after removing AAO membranes. Thanks to the low divergence of the incident metal beam, the shape and arrangement of Ag nanoparticles is well consistent with that of the holes in of the double layer AAO. If the holes of the two membrane are well aligned, the metal nanoparticle at the bottom of the holes is circular, and metal nanoparticle “monomers” are formed. In contrast, if the whole pore walls of the upper AAO sits at the center of the holes of the lower AAO (Fig. 1e), metal nanoparticle “dimers” are obtained (Fig. 1h). Similarly, if the cross corners of the upper AAO sits right at the center of the holes of the lower AAO (Fig. 1f), metal nanoparticle “trimers” are obtained (Fig. 1i). Rotating 30° clockwise relatively, monomers, dimers and trimers form simultaneously. Fig. 1j shows a typical pattern. It looks like a flower.

The low-magnification top-view SEM image of single layer AAO membrane is shown in Fig. S3a. Generally, the shape of the pores of AAO membrane formed in oxalic acid is round after being widened mildly in diluted H_3PO_4.[4] However, in this work, the pores have a hexagonal shape with round corners. This is caused by the duplex structure of the pore wall of AAO. The pore wall has a bilayer structure in terms of chemical composition: relatively pure inner wall with a hexagonal-like shape, and anion contaminated outer wall. For a detailed description, the readers are referred to excellent study by Thompson *et. al.* and Han *et. al.*[5,6] During wet-chemical etching, pore wall oxide in the early stage is etched at a higher rate. This can be attributed to the less dense outer pore wall oxide due to the incorporation of anionic species, as compared to the relatively pure nature of the inner pore wall oxide.[7] The thickness of AAO membrane is ~120 nm. Despite the high aspect ratio of about 12, the pore walls remain upright due to the sufficient mechanical strength of AAO. The main advantages of this transfer and nanoparticle patterning approach are the variability of substrates, the high throughput large-area capability, and the tunability of the nanoparticle size. Any substrates which are stable at 400 ^oC in N_2 for 10 min (e.g. Si, fused silica, glass) can be used in this technique.

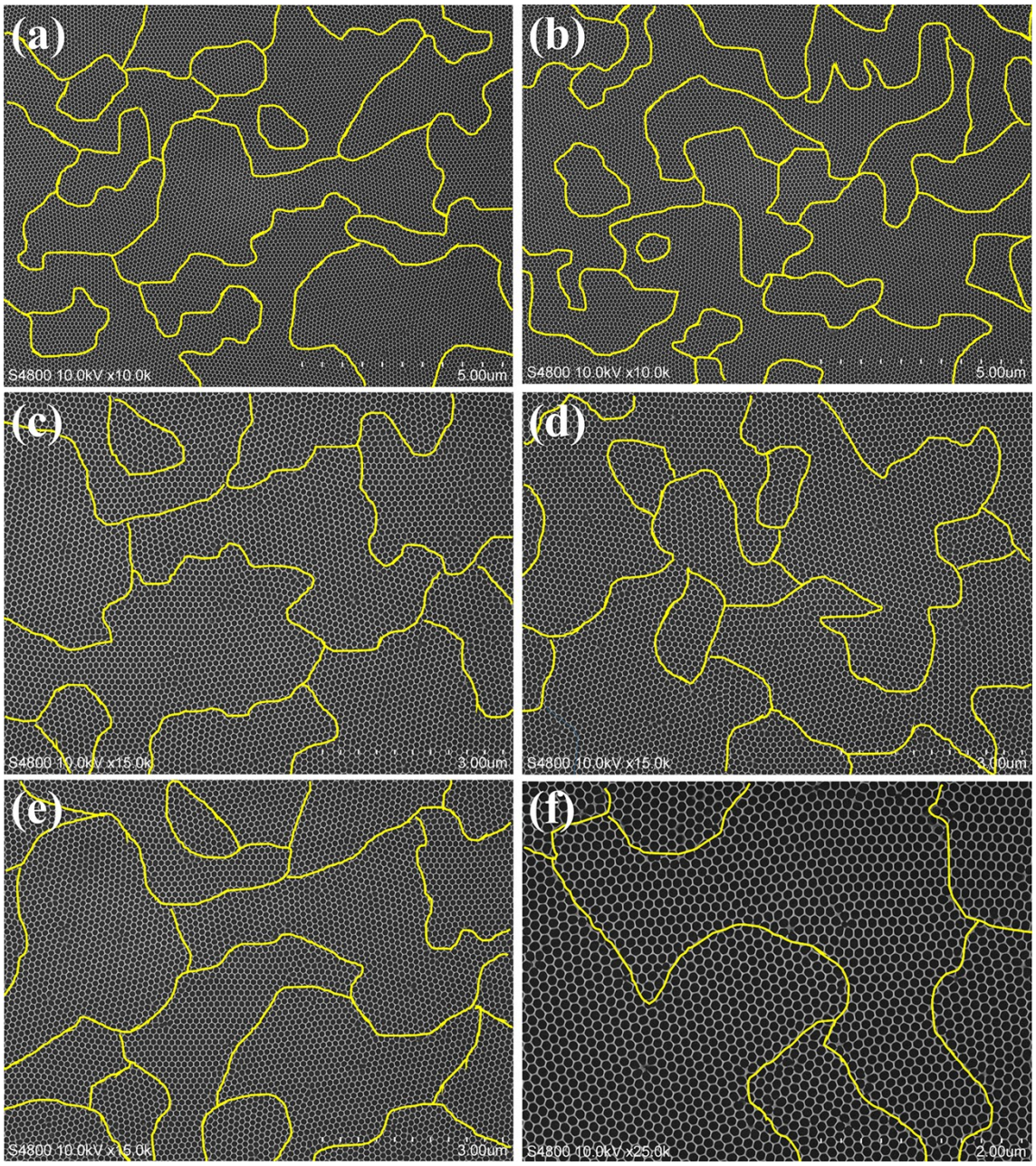

Fig. S4 SEM images of single layer AAO membranes at six different sites of the sample. The pore configurations contain many perfectly ordered domains. Within the domains, hexagonal pore arrangements with the same orientation. The domain boundaries are shown in yellow lines. The ordered range is 1~5 μm for each domain.

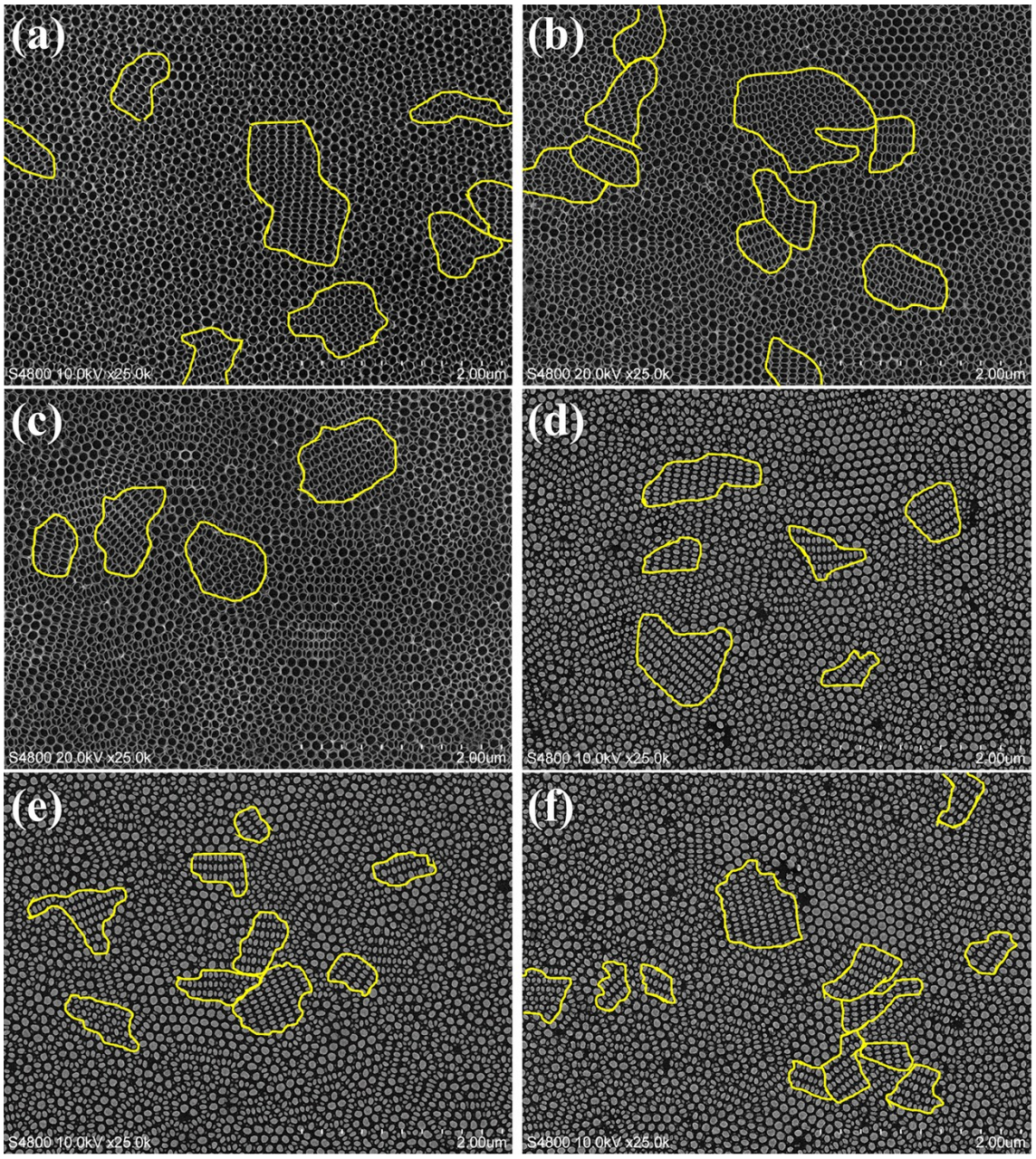

Fig. S5 SEM images of (a-c) double layer AAO membranes and (d-f) Ag nanoparticle arrays fabricated by double layer AAO at different sites of the sample. Some selected domain boundaries are shown in yellow lines. The ordered range is 0.5~1.5 μm for each domain.

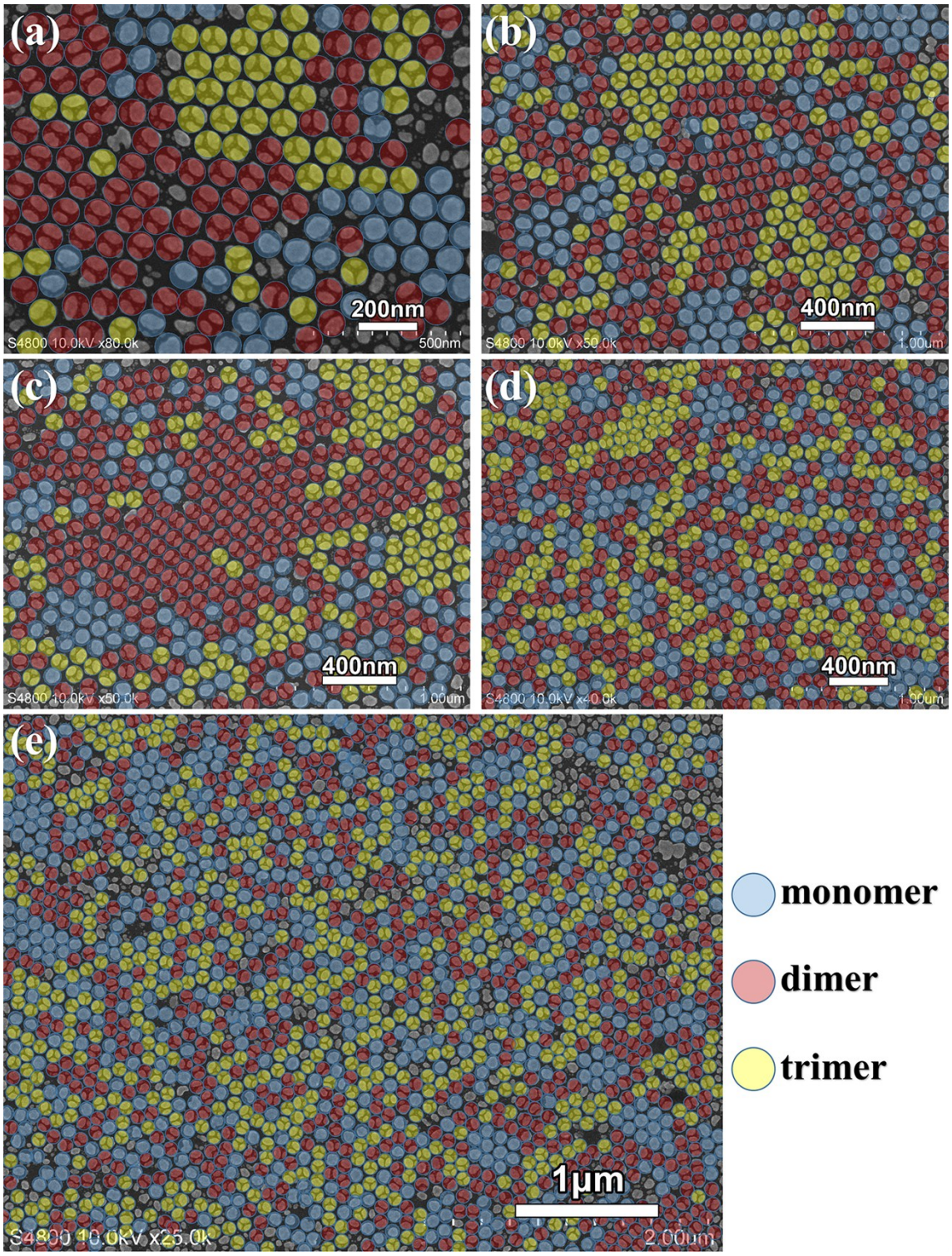

Fig. S6 Statistical appearance probability of monomer, dimer and trimer. Five SEM images at different sites of the sample are selected. Monomers, dimers and trimers are marked by blue, red and yellow semitransparent circles, respectively. The total area of the five images is ~38.15 μm^2. The total number of monomer, dimer and trimer in the images are 909, 1547 and 1145, respectively. The appearance probability of monomer, dimer and trimer are 25.2%, 43%

and 31.8%. Since there are one ~5 nm gap in the dimer and three ~5 nm gaps in the trimer, the total small gap (~5 nm) density is ~130.6 μm^{-2}.

Raman spectra.

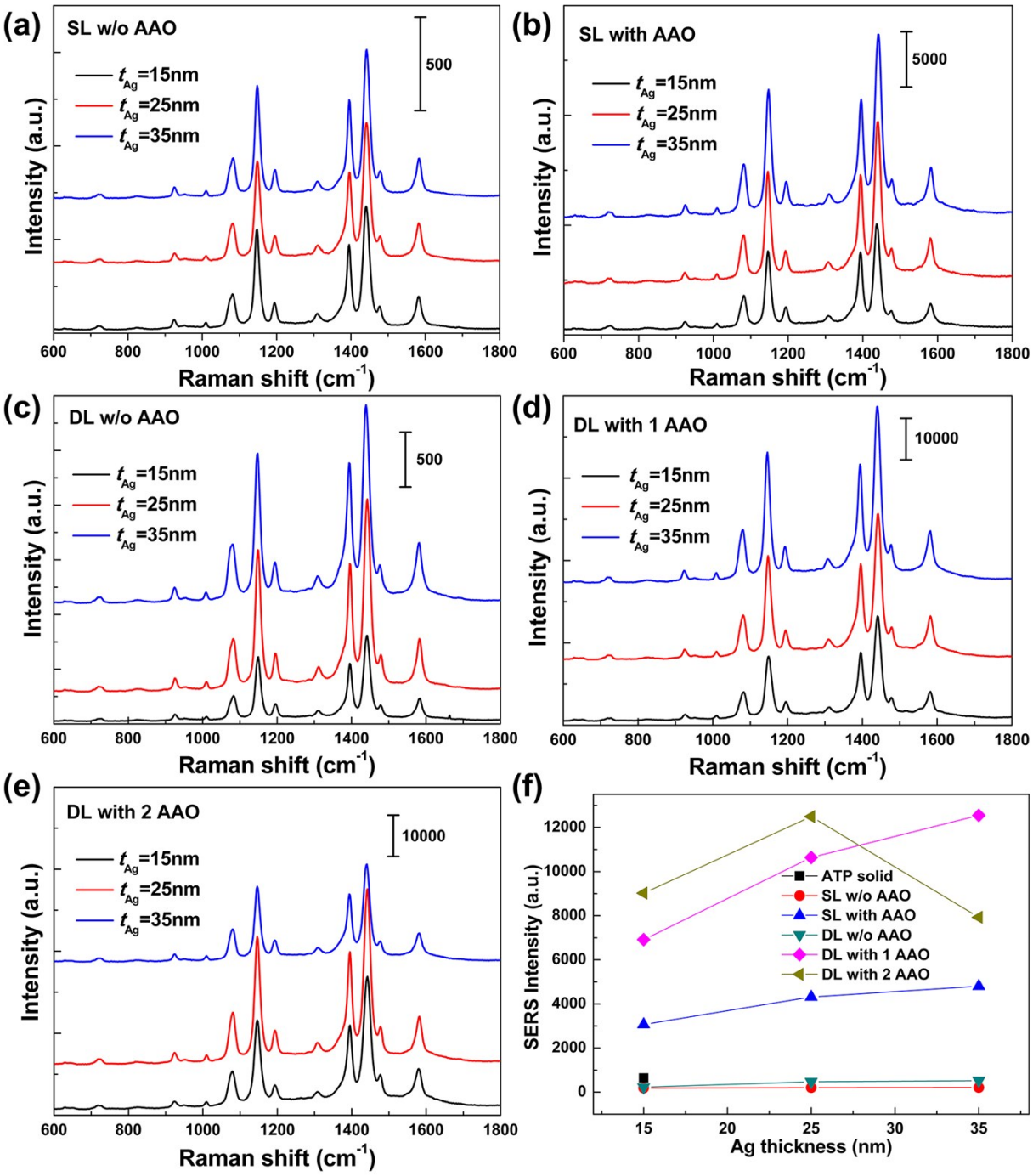

Fig. S7 (a-e) SERS spectra of 4-ATP on Ag nanostructures with different Ag thickness: (a) Ag nanoparticles fabricated by single layer AAO, and the membrane was removed (SL w/o AAO); (b) Ag nanoparticles fabricated by single layer AAO, and the membrane was not removed (SL with AAO); (c) Ag nanoparticles fabricated by double layer AAO, and the membranes was removed (DL w/o AAO); (d) Ag nanoparticles fabricated by double layer

AAO, and the top layer membrane was removed (DL with 1 AAO); (e) Ag nanoparticles fabricated by double layer AAO, and the two layer membranes were not removed (DL with 2 AAO). Here, t_{Ag} is Ag deposition thicknesses. (f) Comparison of the Raman intensity around 1081 cm^{-1} for Ag nanostructures and 1093 cm^{-1} for 4-ATP solid.

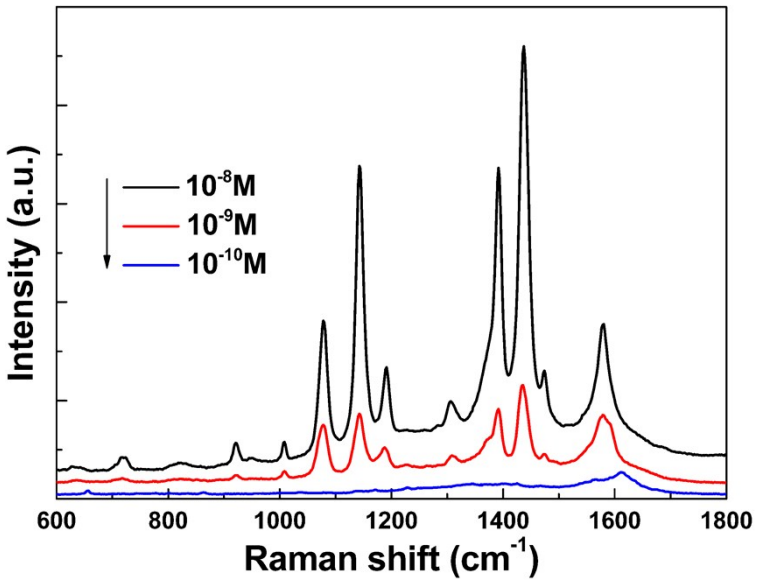

Fig. S8 Concentration-dependent SERS spectra for substrate fabricated by double-layer AAO membranes (DL with 2 layer AAO) with Ag deposition thickness of 25 nm. The concentrations of 4-ATP are 10^{-8}, 10^{-9}, 10^{-10} mol/L. Specifically, the samples for SERS measurements were prepared by depositing 10 μL of ethanol solutions from 10^{-8} to 10^{-10} M on the Ag nanostructures. For the minimal 4-ATP concentration, 10^{-10} M, the SERS peaks cannot be resolved.

EF Calculation details

Table S1 Raman intensity around 1081 cm^{-1} (for Ag nanostructures) and 1093 cm^{-1} (for ATP solid).

	Raman intensity (a.u.)					
t_{Ag} (nm)	ATP solid	SL w/o AAO	SL with AAO	DL w/o AAO	DL with 1 layer AAO	DL with 2 layer AAO
15		188	3068	228	6890	9025
25	644	207	4318	472	10615	12495
35		212	4804	524	12748	7929

Table S2 Comparison of SERS results among different Ag nanostructures.

Structure	Rectangular Ag nanorods	Ag dendrites	SiO_2−Ag nanocap arrays	DL with 2 layer AAO
Probe Molecule	4-ATP	4-ATP	4-ATP	4-ATP
Excitation laser	514 nm	514 nm	514 nm	514 nm
Penetration depth	2 μm	2 μm	19 μm	2 μm
Detection limit	-	-	10^{-7} M	10^{-9} M
I_{SERS}/ I_{bulk}	2.5	2	7.86	19.4
EF	5.06×10^4	5.78×10^3	4.41×10^5	4.41×10^4
Reference	[8]	[9]	[10]	This work

The EF is calculated using the expression: EF = (I_{SERS}/N_{SERS}) / (I_{bulk}/N_{bulk}), where I_{SERS} stands for the intensity of the band at 1081 cm^{-1} in the SERS spectrum of 4-ATP absorbed on Ag nanoparticles and I_{bulk} for that of the band at 1093 cm^{-1} assigned to solid sample. N_{SERS} and N_{bulk} are the number of 4-ATP molecules adsorbed on the SERS substrate and bulk molecules illuminated by the laser, respectively. Here the Ag deposition thickness is 25nm. $N_{SERS} = N_d A_{laser} A_N/\sigma$, where N_d is the number density of the Ag nanoparticles, A_{laser} is the area of the focal spot of laser, A_N is the footprint area of Ag nanoparticles, and σ is the surface area occupied by a single 4-ATP adsorbed on the substrate. N_d and A_N can be obtained from the SEM images, and A_{laser} can be obtained from the diameter of the laser spot (~1 μm). σ is estimated to be 0.20 nm^2.[11] Then the total number of surface adsorbed molecules (N_{SERS}) within the illuminated laser spot can be estimated as list in Table S1. $N_{bulk}=\rho A_{laser} h N_A/M$, where ρ is the density of 4-ATP in the solid state (1.18 g/cm^3), h is the penetration depth (~2 μm) of the focused laser beam in the experiment, and M is the molecular weight (125.19 g/mol). N_{bulk} is calculated to be about 8.91×10^9. The intensities of at 1081 cm^{-1} (curve 1-5) and 1093 cm^{-1} (ATP solid) in Fig. 3 are list in Table S1. The calculated EF results are list in Table 1. The SERS result of this work is compared with other Ag nanostructures reported in the literatures as shown in Table S2. It is worth to point out that the calculation details of these works are quite different. Major variation comes from the determination of the number of molecule absorbed and the choice of penetration depth. Some authors chose penetration depth from 2 μm to 20 μm (Table S2), which should also be take into account when compare different works.

Single-layer AAO mask for comparison.

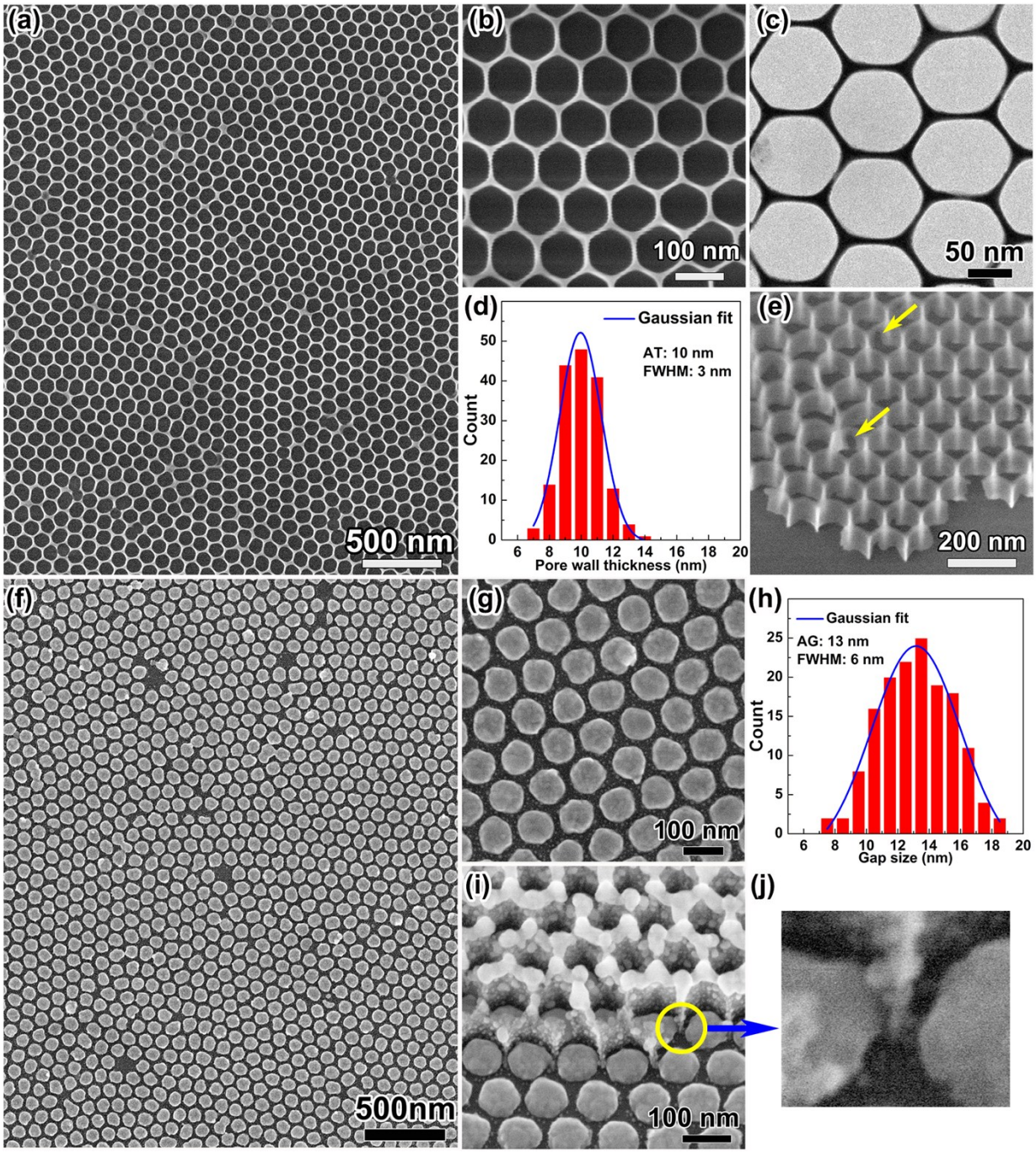

Fig. S9 (a) Low-magnification top-view SEM image of AAO membrane. The center-to-center distance is ~100 nm. (b) A close-up view of the membrane in panel a, showing the detailed shape of the pores. (c) TEM image of the membrane. (d) Histogram and Gaussian fit curve of the pore wall thickness. The blue line corresponds to a Gaussian fit of the experimental data. AT means average pore wall thickness. FWHM refers to half-peak width of the Gaussian fit. (e) 30°-tilted-view SEM image of AAO membrane. The arrows are pointing at the partly broken walls. (f) Low-magnification SEM image showing a large area Ag nanoparticle arrays. The thickness of Ag is 35 nm. (g) A close-up view of Ag nanoparticles. (h) Histogram and

Gaussian fit curve of the gap sizes between neighboring Ag nanoparticles. AG is average gap size. (i) 30°-tilted-view SEM image of Ag nanoparticle arrays with part of AAO membrane remaining.

3D model for simulations.

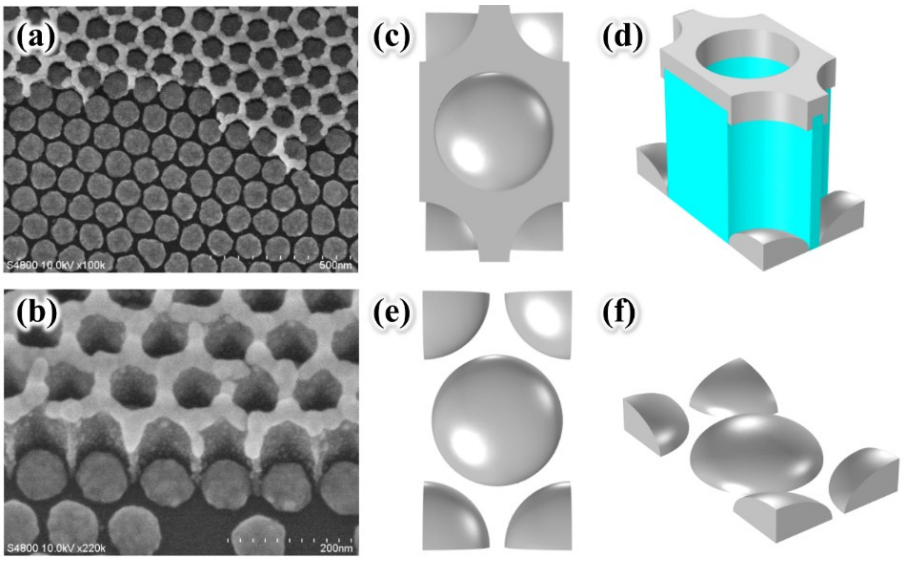

Fig. S10 (a,b) SEM images of Ag nanostructure fabricated by single layer AAO membrane, AAO is partly remained. 3D model in calculation for Ag nanostructures fabricated by single layer AAO (c,d) with and (e,f) without the membrane. t_{Ag}=25 nm.

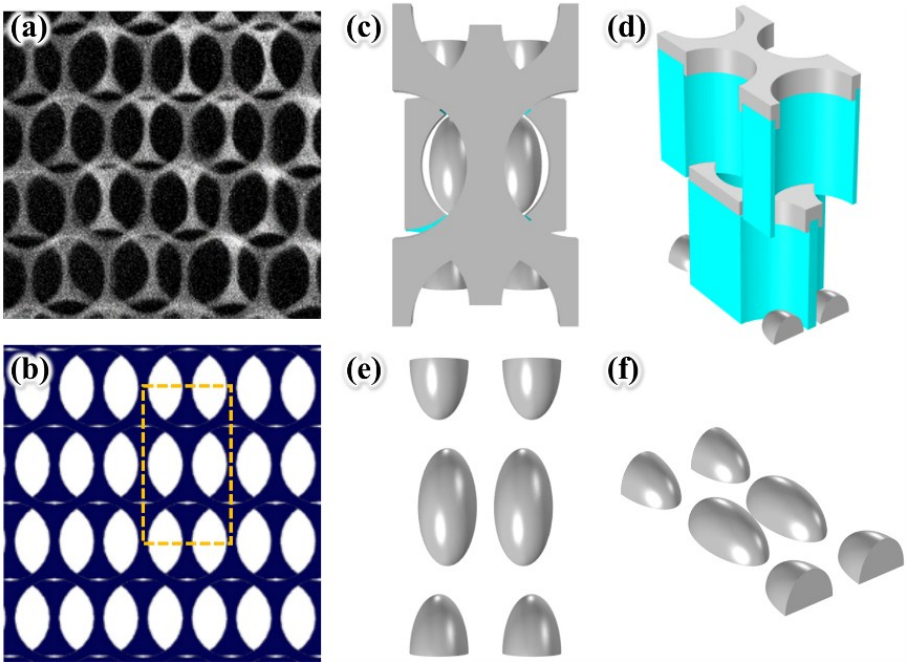

Fig. S11 (a) SEM image and (b) schematic diagram of stacked double layer AAO membrane (type A). 3D model in calculation for Ag nanostructures fabricated by single layer AAO (c,d) with and (e,f) without the membrane. t_{Ag} = 25 nm.

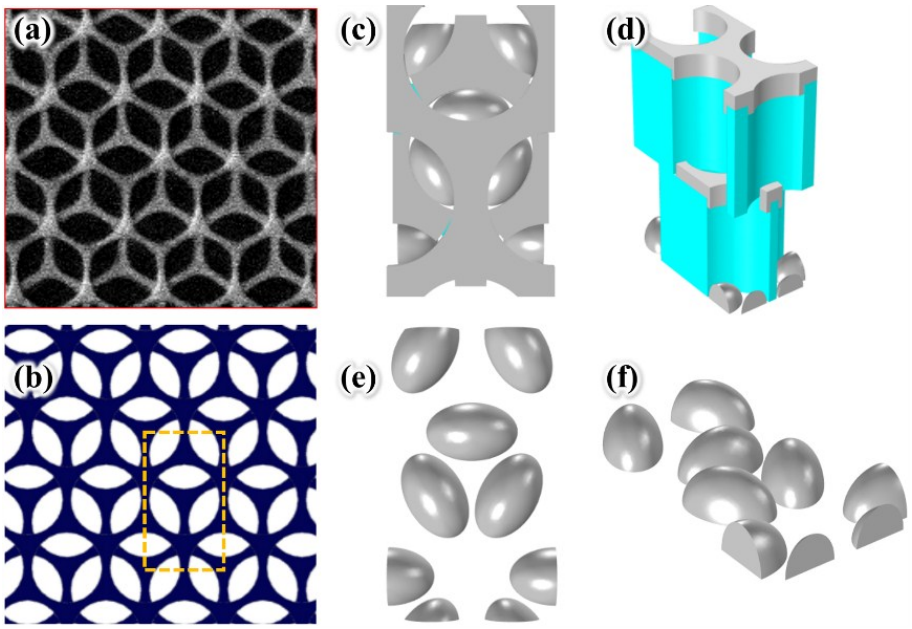

Fig. S12 (a) SEM image and (b) schematic diagram of stacked double layer AAO membrane (type B). 3D model in calculation for Ag nanostructures fabricated by single layer AAO (c,d) with and (e,f) without the membrane. t_{Ag}=25nm.

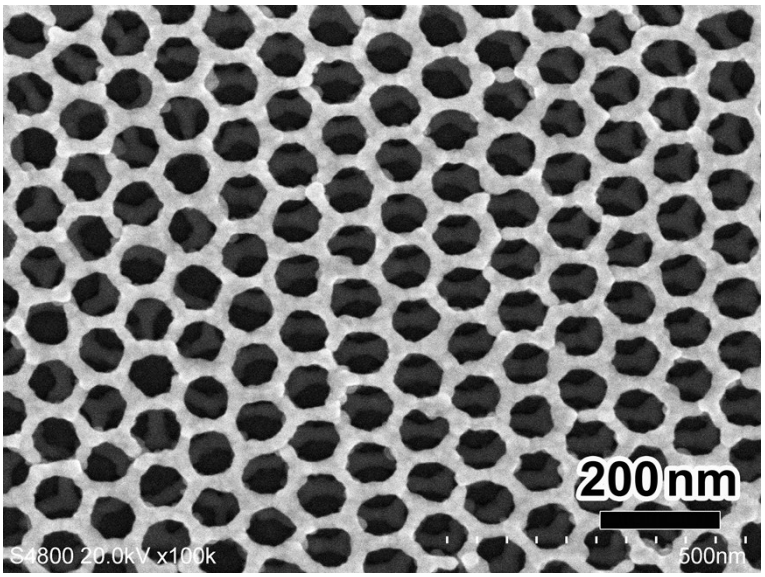

Fig. S13 Top view SEM image of stacked double layer AAO membrane after 25 nm Ag deposition.

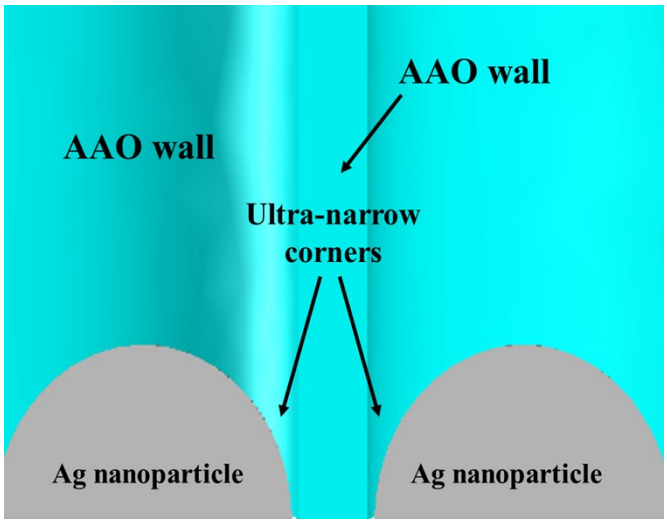

Fig. S14 The ultra-narrow corners formed between the outer surface of Ag particles and nearby AAO wall.

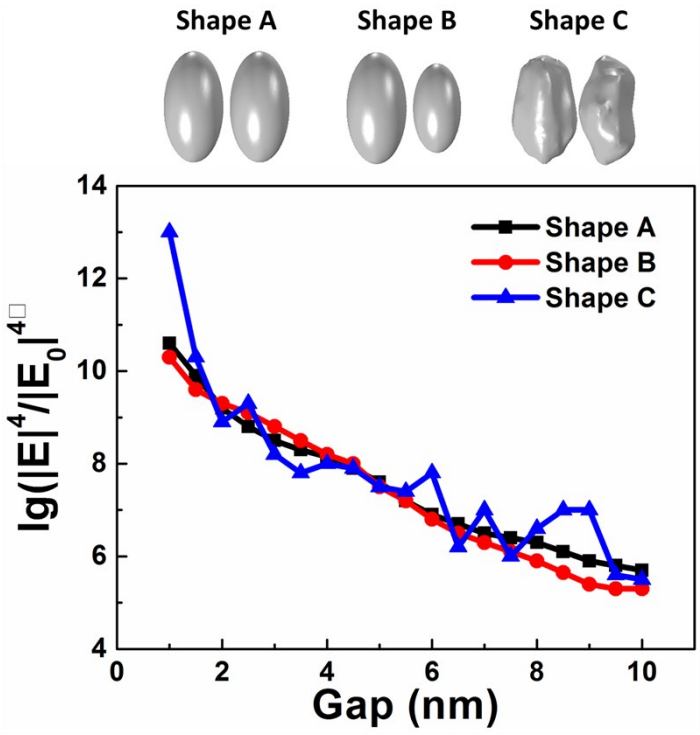

Fig. S15 Three types of dimers in calculations are considered, i.e. symmetric dimer, asymmetric dimer and dimers consisted of random shaped particles. Although the particle size is not completely uniform, this does not affect the enhancement because the electric field enhancement mainly depends on the gap size.

References:

1 Z. L. Huang, G. W. Meng, Q. Huang, Y. J. Yang, C. H. Zhu, C. L. Tang, *Adv. Mater.* 2010, **22**, 4136.

2 Z. B. Zhan, Y. Lei, *ACS Nano.* 2014, **8**, 3862.

3 W. R. Zeng, S. F. Li, W. K. Chow, *J. Fire Sci.* 2002, **20**, 297.

4 C. C. Zhao, Y. Zhu, Y. Q. Su, Z. Y. Guan, A. Q. Chen, X. Ji, X. C. Gui, R. Xiang, Z. K. Tang, *Adv. Opt. Mater.* 2015, **3**, 248.

5 H. Han, S. J. Park, J. S. Jang, H. Ryu, K. J. Kim, S. Baik, W. Lee, *ACS Appl. Mater. Interfaces* 2013, **5**, 3441.

6 G. E.Thompson, G. C. Wood, *Nature* 1981, 290, 230.

7 W. Lee, S. J. Park, *Chem. Rev.* 2014, **114**, 7487.

8 S. J. Guo, S. J. Dong, E. K. Wang, *Cryst. Growth Des.* 2009, **9**, 372.

9 L. Wang, H. L. Li, J. Q. Tian, X. P. Sun, *ACS Appl. Mater. Interfaces* 2010, **2**, 2987.

10 Y. X. Wang, X. Y. Zhao, L. Chen, S. Chen, M. B. Wei, M. Gao, Y. Zhao, C. Wang, X. Qu, Y. J. Zhang, J. H. Yang, *Langmuir* 2014, **30**, 15285.

11 S. M. Zhu, C. Z. Fan, J. Q. Wang, J. N. He, E. J. Liang, M. J. Chao, *J. Appl. Phys.* 2014, **116**, 044312.